Geochemical Perspectives Letters

A secretive mechanical exchange between mantle and crustal volatiles revealed by helium isotopes in ^{13}C-depleted diamonds

S. Mikhail[1*], J.C. Crosby[1+], F.M. Stuart[2], L. DiNicola[2], F.A.J. Abernethy[3]

OPEN ACCESS

doi: 10.7185/geochemlet.1923

Abstract

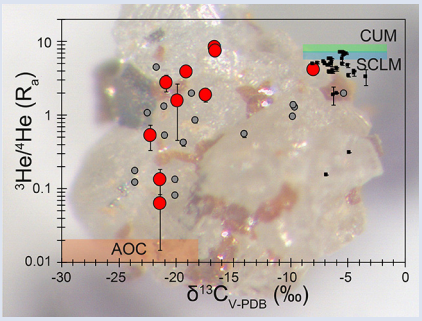

Fluid inclusions trapped in fast-growing diamonds provide a unique opportunity to examine the origin of diamonds, and the conditions under which they formed. Eclogitic to websteritic diamondites from southern Africa show ^{13}C-depletion and ^{15}N-enrichment relative to mantle values (δ^{13}C = -4.3 to -22.2 ‰ and δ^{15}N = -4.9 to +23.2 ‰). In contrast the ^{3}He/^{4}He of the trapped fluids have a strong mantle signature, one sample has the highest value so far recorded for African diamonds (8.5 ± 0.4 R$_a$). We find no evidence for deep mantle He in these diamondites, or indeed in any diamonds from southern Africa. A correlation between ^{3}He/^{4}He ratios and ^{3}He concentration suggests that the low ^{3}He/^{4}He are largely the result of ingrowth of radiogenic ^{4}He in the trapped fluids since diamond formation. The He-C-N isotope systematics can be best described by mixing between fluid released from subducted altered oceanic crust and mantle volatiles. The high ^{3}He/^{4}He of low δ^{13}C diamondites reflects the high ^{3}He concentration in the mantle fluids relative to the slab-derived fluids. The presence of post-crystallisation ^{4}He in the fluids means that all ^{3}He/^{4}He are minima, which in turn implies that the slab-derived carbon has a sedimentary organic origin. In short, although carbon and nitrogen stable isotope data show strong evidence for crustal sources for diamond-formation, helium isotopes reveal an unambiguous mantle component hidden within a strongly ^{13}C-depleted system.

Received 23 April 2019 | Accepted 28 August 2019 | Published 10 October 2019

Introduction

Placing diamond-formation into context of large scale tectonothermal processes, such as subduction and plume-lithosphere interaction, is fundamental to understanding the deep terrestrial carbon cycle (Shirey *et al.*, 2013). Diamond is a chemically simple mineral comprised largely of C and trace N (~0.025 %) incorporated as single nitrogen atoms substituting for carbon (Kaiser and Bond, 1959). The origin of diamond-forming fluids is commonly addressed using the stable isotope values of carbon and nitrogen, where coupled δ^{13}C-δ^{15}N values can indicate diamond growth from mantle-derived fluids (Cartigny *et al.*, 2014). However, many datasets require the contribution of crustal sources for the C and/or N, such as eclogitic diamonds from Dachine (Smith *et al.*, 2016). Sometimes, C-N isotope systematics do not fully resolve the origin of the diamond-forming fluids. For instance, eclogitic diamonds from Jwaneng (Cartigny *et al.*, 1998) and Orapa (Cartigny *et al.*, 1999) show crust-like low δ^{13}C values yet have mantle-like negative δ^{15}N values (Fig. 1), and C and N isotope systems can be decoupled during diamond-formation (Mikhail *et al.*, 2014; Hogberg *et al.*, 2016).

Diamonds can trap fluid during their growth, either along the diamond fibres, between interlocking polycrystalline grains, and surrounding diamond-hosted mineral inclusions (Navon *et al.*, 1988; Jacob *et al.*, 2014). As well as providing the only direct samples of metasomatic fluids from the mantle (Weiss *et al.*, 2015), the trapped fluids enable the application of noble gas isotope tracers to resolve the origin of diamond-forming fluids (Burgess *et al.*, 1998; Gautheron *et al.*, 2005; Broadley *et al.*, 2018; Timmermann *et al.*, 2018, 2019a,b). Here we combine C-N isotope and nitrogen abundance data from southern African diamondites with He isotope data from micro-inclusions in the same sample to investigate the origin of carbonaceous fluids in the mantle. These new data shed light on the number of discrete sources required for the generation of carbonaceous high-density fluids responsible for diamond-formation in the SCLM.

Samples and Methods

Three main diamond types are recognised; monocrystalline, fibrous and polycrystalline. The latter, also known as diamondites, are a mixture of diamond intergrown with silicates and

1. The School of Earth and Environmental Sciences, University of St. Andrews, UK
2. Isotope Geosciences Unit, Scottish Universities Environmental Research Centre, UK
3. Department of Physical Sciences, The Open University, UK
+ Present address, Department of Earth Science, University of Cambridge, UK
* Corresponding author (email: sm342@st-andrews.ac.uk)

Table 1 Data for southern African diamondites. A full data table including all comparative data is located in the Supplementary Information (Table S-1).

Sample	Location	Para	Minerals	R/Ra	±	^{4}He ccSTP/g	^{3}He ccSTP/g	δ^{13}C (‰)	±	N at.ppm	δ^{15}N (‰)	±
DIA030	SA	W	Gnt	8.5	0.4	1.33 E-07	1.51 E-12	-16.6	0.2	8	+6.4	3.9
DIA053	SA	W	Gnt	2.8	0.7	3.20 E-08	1.18 E-13	-20.8	0.5	56	+2.0	0.7
DIA057B#1	SA			0.1	0.0	6.79 E-07	5.81 E-14	-21.4	0.1	1389		
DIA057B#2	SA			0.1	0.1	6.90 E-07	1.25 E-13	-21.4	0.1	1389		
DIA058B	SA	E	Gnt	3.9	0.2	7.42 E-08	3.84 E-13	-19.1	0.1			
DIA059	SA	W	Gnt	0.5	0.2	1.42 E-07	1.01 E-13	-22.2	0.3	13	+5.3	6.1
DIA073B	SA	W	Gnt	1.9	0.4	8.71 E-08	2.21 E-13	-17.4	0.1	2812	+6.9	0.5
DIA077	SA			7.4	0.5	1.44 E-07	1.43 E-12					
ORF9	Orapa	W	Gnt			2.44 E-08		-5.3	0.1			
ORF12	Orapa					6.72 E-08						
ORF19	Orapa	E	Gnt	4.2	2.7	9.02 E-08	5.11 E-13	-8.0	0.1	255	+5.8	0.1
ORF26#1	Orapa	P + E	Cpx + Gnt			4.22 E-09		-14.6	0.2	38	-4.8	2.2
ORF26#2	Orapa	P + E	Cpx + Gnt					-17.8	0.2	19	+23.2	6.6
ORF28#1	Orapa					5.37 E-08		-4.3	0.1	775	+2.9	0.2
ORF28#2	Orapa							-4.9	0.2	52	+19.7	0.6
ORF41	Orapa					7.77 E-08		-14.8	0.3	1146	+14.7	0.2
ORF57	Orapa	E	Gnt	7.5	0.7	2.24 E-07	2.26 E-12	-16.6	0.2	17	+18.4	3.0
ORF60	Orapa		Chromite					-6.5	0.1	1054	+12.1	0.2
ORF91	Orapa							-20.3	0.3	401	+4.4	0.3
ORF143	Orapa	E	Gnt	1.6	1.1	1.03 E-07	2.17 E-13	-19.9	0.2	647	+10.0	0.2

Abbreviations: W = websteritic, P = peridotitic, E = eclogitic, Gnt = garnet, Cpx = clinopyroxene, SA = southern Africa.

oxides (Kurat and Dobosi, 2000). Seventeen diamondites in this study are from two collections, the Orapa and the southern African diamondites (n = 10 and 7 respectively; Table 1). These samples are described in detail elsewhere (Kurat and Dobosi., 2000; Mikhail *et al.*, 2019; Supplementary Information). The δ^{13}C, δ^{15}N values and N concentrations were obtained using the automated and custom-made Finesse system at the Open University following the method outlined in Mikhail *et al.* (2014). The helium isotope composition of trapped fluids released by *in vacuo* crushing were determined using a ThermoFisher Scientific Helix-SFT mass spectrometer at the Scottish Universities Environmental Research Centre (Carracedo *et al.*, 2019). These data are provided in Table 1.

Carbon and Nitrogen Geochemistry

δ^{13}C values range from -4.3 to -22.2 ‰ and δ^{15}N range from -4.9 to +23.2 ‰ (Fig. 1). Although they overlap, the southern Africa diamondites have lower mean δ^{13}C (-19.8 *vs.* -12.1 ‰) and higher average δ^{15}N values (+10.6 *vs.* +5.2 ‰) than the Orapa diamondites. There is no systematic relationship between C or N isotope values and the silicate paragenesis, consistent with previous observations (Mikhail *et al.*, 2019). Although mantle-like C and N isotope values are recorded, no sample plots in the mantle field (Fig. 1). Diamondites show ^{13}C-depletion and ^{15}N-enrichment relative to mantle values. The Orapa diamondites have a more pronounced ^{13}C-depletion and ^{15}N-enrichment when compared to the eclogitic and peridotitic monocrystalline diamonds from the same kimberlite (Fig. 1). These data indicate crustal fluids sourced from subducted oceanic sediments or altered oceanic crust (Thomazo *et al.*, 2009). Nitrogen concentrations range from 8–1389 ppm and do not correlate with δ^{13}C or δ^{15}N, consistent with previous observations (Mikhail *et al.*, 2013, 2014, 2019). The lack of correlation between nitrogen concentrations with δ^{13}C or δ^{15}N in both datasets may reflect multiple diamond forming events, or isotopic heterogeneity in the source.

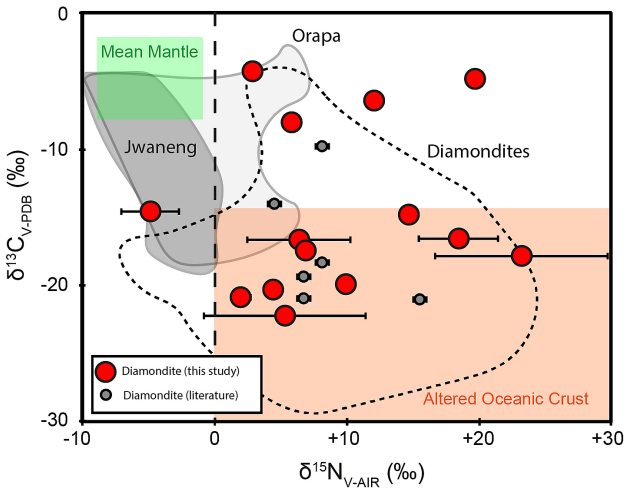

Figure 1 New C and N isotope data for southern African diamondites (red circles) and literature data (grey circles: Gautheron *et al.*, 2005; Burgess *et al.*, 1998) Fields are shown for other diamondites (Mikhail *et al.*, 2013), eclogitic monocrystalline diamonds from Jwaneng (Cartigny *et al.*, 1998) and Orapa (Cartigny *et al.*, 1999), the mean mantle and altered oceanic crustal material (Cartigny *et al.*, 2014).

Helium Isotopes

The ^{3}He/^{4}He ratios range from 0.06 to 8.3 R_a, overlapping, but extending, the range previously measured in southern Africa diamondites (Fig. 2a). The highest ^{3}He/^{4}He in these

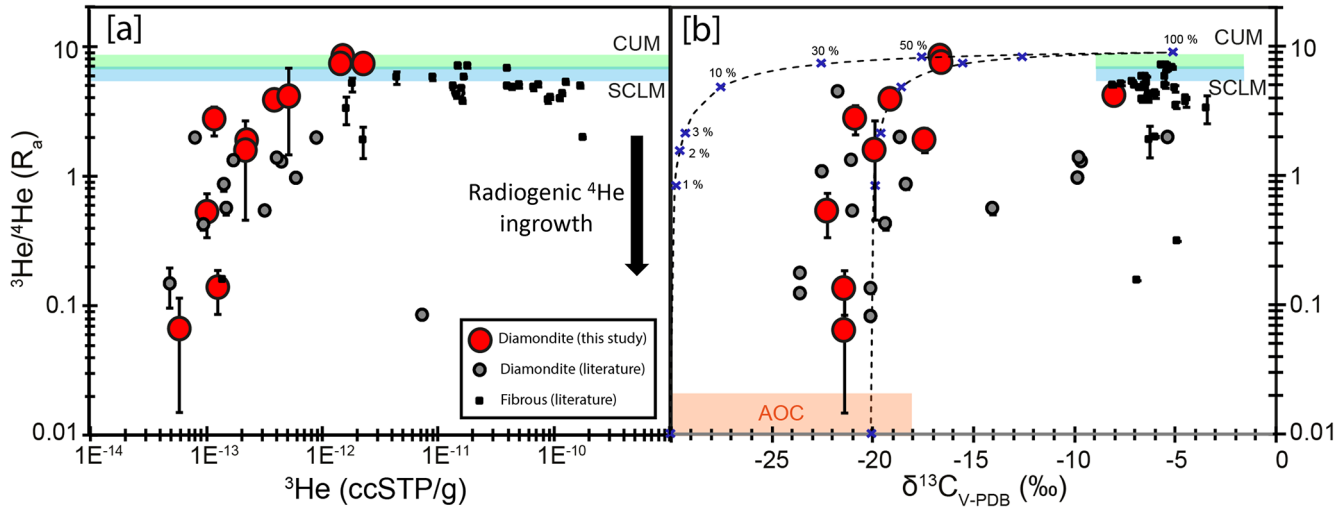

Figure 2 **(a)** Helium isotope systematics of fluids released by *in vacuo* crushing of diamondites. The ^{3}He/^{4}He of modern the convecting upper mantle (CUM) and the sub-continental lithospheric mantle (SCLM) are shown for reference. **(b)** Carbon-helium isotope systematics of southern African diamondites and fibrous diamonds from across southern Africa. The mixing lines are plotted between mantle and crustal fluid sources, the crosses refer to percent of mantle fluid component. The mixing lines plotted in Figure 2b are hyperbolic as $[^4He]_{mantle}/[^4He]_{crust}$ is assumed to be 10. Comparative data are from Burgess *et al.* (1998), Gautheron *et al.* (2005) and Timmermann *et al.* (2018, 2019a).

diamondites (8.3 ± 0.4 R_a) exceeds the highest ratios measured in all other diamondites and fibrous diamonds from southern Africa (Fig. 2a). It is higher than values typical of SCLM (6.1 ± 1 R_a; Gautheron *et al.*, 2005) and modern kimberlite from southern Africa (4.2 R_a; Brown *et al.*, 2012), and overlaps the present day convecting upper mantle (8 ± 1 R_a; Graham *et al.*, 2014).

The southern Africa diamondites formed between kimberlite emplacement and craton stabilisation (91 to >3000 Ma; Gurney *et al.*, 2010). The highly aggregated nitrogen in diamondites is consistent with long mantle residence times (Mikhail *et al.*, 2019), which implies ages far greater than 91 Ma. This leaves open the likelihood that ^{4}He produced by alpha decay of U and Th in the fluid, or recoil of ^{4}He into the fluids, has decreased the ^{3}He/^{4}He (Timmermann *et al.*, 2019a). A strong relationship between ^{3}He/^{4}He and ^{3}He concentration is apparent from Figure 2a and reflects radiogenic ^{4}He production since the fluids were trapped in the diamond. In this case, all ^{3}He/^{4}He ratios are minimum values, although it appears that diamonds with >1 x 10^{-12} ccSTP ^{3}He/g are largely immune to the effect based on Figure 2a. The diamonds studied here are not alluvial, ruling out cosmogenic ^{3}He implantation during surface exposure (*e.g.*, Yakubovich *et al.*, 2019).

Tracing the Origin of Diamondite-forming Volatiles

Mixing lines in Figure 2b are drawn between oceanic crust-derived fluids with $\delta^{13}C$ = -20 and -30 ‰, and ^{3}He/^{4}He = 0.01 R_a, and mantle-derived fluids with $\delta^{13}C$ = -5 ‰ and ^{3}He/^{4}He = 9 R_a. The mantle ^{3}He/^{4}He end member is slightly higher than the present day upper asthenosphere and lithosphere mantle values, reflecting the temporal evolution of ^{3}He/^{4}He in the mantle (Porcelli and Elliot, 2008).

The spread of data can be explained by mixing between He-rich, high ^{3}He/^{4}He mantle source ($\delta^{13}C$ = -5 ‰) and a He-poor, low ^{3}He/^{4}He crustal component ($\delta^{13}C$ between -15 and -25 ‰). This is strongly supported by the ^{15}N-enrichment in the ^{13}C-depleted samples which best matches altered oceanic crust (Cartigny *et al.*, 2014) or organic material hosted in sedimentary rocks (Thomazo *et al.*, 2009). Furthermore, the prevalence of eclogitic to websteritic silicate inclusions/intergrowths in these diamondites further supports a recycled basaltic component (Mikhail *et al.*, 2019). These observations contrast strongly with the fibrous diamonds which, although they also contain a high density of trapped fluids with evidence of recycled material based on lithophile element geochemistry and Sr-isotopes (Weiss *et al.*, 2015), they commonly show C and N isotope values that are indistinguishable from mantle values (see Fig. 2a,b). Despite significantly lower ^{3}He concentrations, they are thus more likely to be affected by radiogenic ^{4}He ingrowth; the highest ^{3}He/^{4}He southern African diamondites are higher than the highest values measured in fibrous diamonds from southern Africa (Fig. 2a). This suggests that there is no genetic link between the fibrous diamonds and diamondites, and they likely formed in different mantle domains or from isotopically distinct sources.

A mantle origin for the helium trapped in the diamondite fluids is incontrovertible (Fig. 2a), but the incorporation mechanism(s) for He into the high density fluids (HDF) is less clear. Possible mechanisms include the assimilation of He from grain boundaries or small volume mantle melts initiated by the expulsion of slab-derived fluids into the mantle wedge or SCLM. Resolving the origin of the mantle He is hampered by the post-formation ingrowth of radiogenic ^{4}He, and because the ^{3}He/^{4}He ratio of the mantle has reduced over time (*e.g.*, Porcelli and Elliot, 2008). The uncertainty in the diamond age and the He isotope evolution of the mantle makes drawing firm conclusions regarding the source of the mantle He problematic. One prevailing view posits that the southern African kimberlites originate at the edges of large heterogeneities at the core-mantle boundary (Torsvik *et al.*, 2010). This should be evident from high ^{3}He/^{4}He (*e.g.*, Stuart *et al.*, 2003) in kimberlitic fluids. In contrast to Brazilian diamonds (Timmerman *et al.*, 2019b), the absence of ^{3}He/^{4}He above Phanerozoic upper mantle values in fluid-rich diamonds from southern Africa rules likely reflects the formation of the diamonds prior to the generation of the kimberlite melts, and post-formation isolation from kimberlitic fluids. Furthermore, it is conceivable that high ^{3}He/^{4}He ratios (>10 R_a) in some samples (*e.g.*, Siberian fibrous diamonds; Broadley *et al.*, 2018) might reflect the higher ^{3}He/^{4}He of the ancient mantle, as opposed to evidence

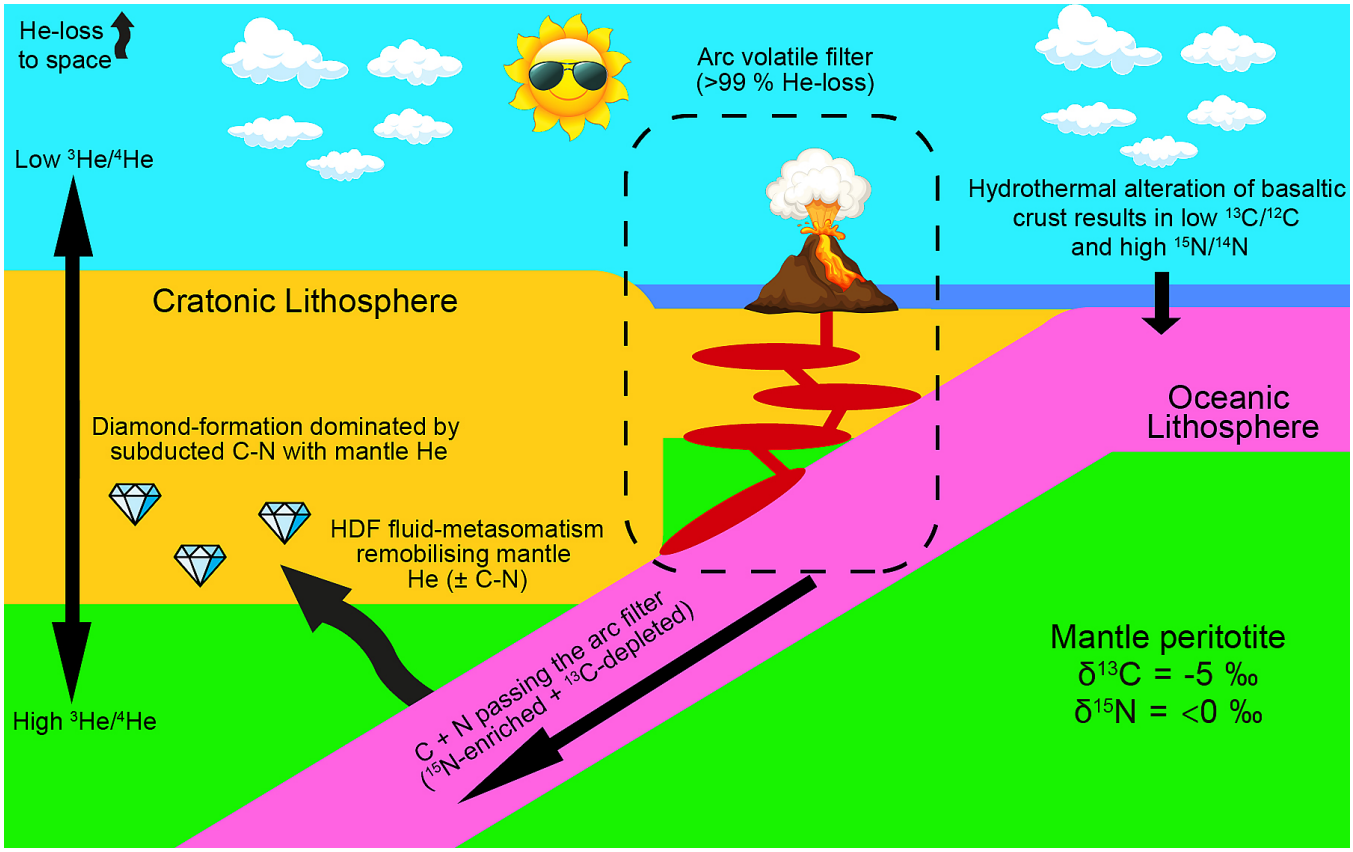

Figure 3 Cartoon illustrating the model discussed in the text. Not to scale.

for the role of mantle plumes in the generation of shallow diamonds. While the highest diamondite ^{3}He/^{4}He ratios are above modern SCLM values, they do not allow a distinction to be made between an ancient sub-continental lithospheric or a convecting upper asthenospheric mantle source. That said, the absence of ^{3}He/^{4}He above Phanerozoic upper mantle values in fluid-rich diamonds from all southern Africa rules out a requirement for deep mantle fluids in the generation of diamonds in the SCLM. Diamondites from southern Africa crystallised from HDFs where the C originates from crustal and mantle sources, the N is mostly slab derived, likely from a subducted sedimentary organic component, but the He is largely derived from the upper mantle.

The carbon and nitrogen isotope data (Fig. 1) are consistent with prevailing models for diamondite-formation, whereby high density fluid from a subducting slab interacts with the SCLM (Mikhail *et al.*, 2013, 2019; Jacob *et al.*, 2000, 2014). Mechanically, this journey provides an opportunity for the exchange of material between a subducted fluid acting as a mobilising agent (HDF) with solid residual mantle rocks (illustrated in Fig. 3). This physical interaction can assimilate mantle volatiles into the HDF resulting in hybridisation (where the HDF is now comprised of subducted + mantle volatiles). If the mantle component in the subduction-derived HDF is small, then the diamond-forming media might not reveal this assimilated mantle component in δ^{13}C-δ^{15}N space (*e.g.*, as shown for most samples in Fig.1). For example, if the subducted carbon has δ^{13}C = -25 ‰ and assimilated 10 % mantle carbon (δ^{13}C = -5 ‰) with most of the nitrogen provided by the subducted source (δ^{15}N > 0 ‰) then the resulting hybrid would have a δ^{13}C value of -23 ‰ and positive δ^{15}N. Such δ^{13}C-δ^{15}N values do not suggest mixing between mantle and crustal volatiles because they are within the range of crustal organic carbon and distinct from the canonical mean mantle values for both δ^{13}C and δ^{15}N (-5 ± 3 ‰; Cartigny *et al.*, 2014; Mikhail *et al.*, 2014). However, if the ^{13}C-depleted HDF assimilated 50 % mantle carbon and 100 % mantle helium, then the resulting hybrid would have a δ^{13}C value of -15 ‰ and ^{3}He/^{4}He > 1 R_a. This scenario matches the data of samples Dia030 (southern Africa) and ORF57 (Orapa) which show elevated ^{3}He/^{4}He ratios of 8.5 and 7.5 Ra with corresponding δ^{13}C values (-16.6 ‰; Fig. 2b).

We argue that the C-N isotope data commonly identify a mix of multiple sources. In the case of the southern African and Orapa diamondites, the δ^{13}C-δ^{15}N systematics reveal that the subducted component dominates over the mantle component (Fig. 1). However, the discrete, but important, mantle component is revealed in the fluid-hosted helium isotope data. The higher ^{3}He concentration of the mantle fluids compared to slab-derived fluids means that the helium isotopes trace small contributions of mantle-derived volatiles better than C or N isotopes. For example, samples DIA058B (southern African) and ORF143 (Orapa) show elevated ^{3}He/^{4}He ratios of 3.9 and 1.6 R_a with correspondingly low δ^{13}C values of -19.1 and -19.9 ‰ (Fig. 2b). Ergo, helium reveals what carbon and nitrogen cannot. When the carbon and nitrogen stable isotope data show strong evidence for crustal sources for diamond formation (Fig. 1), the helium isotopes reveal an unambiguous mantle component hidden within strongly ^{13}C-depleted diamond (Fig. 2b). This observation speaks to the mechanics of fluid migration through the SCLM. Our data require that subducted material percolates though ambient mantle *en route* to the SCLM and results in the mechanical re-mobilisation of primary mantle volatiles (Fig. 3). These data further enhance the notion that the volatile-element components within a diamond-forming HDF do not always share a common origin, and indeed, the C-N-He isotopic systems preserved in mantle diamonds record distinct processes and should not be considered coupled isotopic systems, by default.

Acknowledgements

SM acknowledges support from the National Environmental Research Council (grant no. NE/PO12167/1). We are grateful to Dr. J.J. Gurney, Dr. Gabor Dobosi, and the late Prof. Gero Kurat for sample provisions, and the editorial handling of Prof. Cin-Ty Lee.

Editor: Cin-Ty Lee

Additional Information

Supplementary Information accompanies this letter at http://www.geochemicalperspectivesletters.org/article1923.

Cite this letter as: Mikhail, S., Crosby, J.C., Stuart, F.M., DiNicola, L., Abernathy, F.A.J. (2019) A secretive mechanical exchange between mantle and crustal volatiles revealed by helium isotopes in ^{13}C-depleted diamonds. *Geochem. Persp. Let.* 11, 39–43.

References

Broadley, M.W., Kagi, H., Burgess, R., Zedgenizov, D., Mikhail, S., Almayrac, M., Ragozin, A., Pomazansky, B., Sumino, B. (2018) Plume-lithosphere interaction, and the formation of fibrous diamonds. *Geochemical Perspectives Letters* 8, 26–30.

Brown, R.J., Manya, S., Buisman, I., Fontana, G., Field, M., Mac Niocaill, C.M., Sparks, R.S.J., Stuart, F.M. (2012) Eruption of kimberlite magmas: physical volcanology, geomorphology and age of the youngest kimberlitic volcanoes known on earth (the Upper Pleistocene/ Holocene Igwisi Hills volcanoes, Tanzania). *Bulletin of Volcanology* 74, 1621–1643, doi: 10.1007/s00445-012-0619-8.

Burgess, R., Johnson, L., Mattey, D., Harris, J., Turner, G. (1998) He, Ar and C isotopes in coated and polycrystalline diamonds. *Chemical Geology* 146, 205–217.

Carracedo, A. Rodés, Á., Smellie, J., Stuart, F.M. (2019) Episodic erosion in West Antarctica inferred from cosmogenic ^{3}He and ^{10}Be in olivine from Mount Hampton. *Geomorphology* 327, 438–445.

Cartigny, P., Harris, J.W., Javoy, M. (1998) Eclogitic diamond formation at Jwaneng: no room for a recycled component. *Science* 280, 1421–1424.

Cartigny, P., Harris, J.W., Javoy, M. (1999) Eclogitic, peridotitic and metamorphic diamonds and the problems of carbon recycling—the case of Orapa (Botswana). *7th International Kimberlite Conference Extended Abstracts*, 117–124.

Cartigny, P., Palot, M., Thomassot, E., Harris, J.W. (2014) Diamond formation: A stable isotope perspective. *Annual Reviews of Earth and Planetary Sciences* 42, 699–732.

Gautheron, C., Cartigny, P., Moreira, M., Harris, J.W., Allégre, C. J. (2005) Evidence for a mantle component shown by rare gases, C and N isotopes in polycrystalline diamonds from Orapa (Botswana). *Earth and Planetary Science Letters* 240, 559–572.

Graham, D.W., Hanan, B.B., Hémond, C., Blichert-Toft, J., Albarède, F. (2014) Helium isotopic textures in Earth's upper mantle. *Geochemistry, Geophysics, Geosystems* 15, 2048–2074, doi: 10.1002/2014GC005264.

Gurney, J.J., Helmstaedt, H.H., Richardson, S.H., Shirey, S.B. (2010) Diamonds through time. *Economic Geology* 105, 689–712.

Hogberg, K., Stachel, T., Stern, R.A. (2016) Carbon and nitrogen isotope systematics in diamond: Different sensitivities to isotopic fractionation or a decoupled origin? *Lithos* 265, 16–30.

Jacob, D.E., Viljoen, K.S., Grassineau, N., Jagoutz, E. (2000) Remobilization in the cratonic lithosphere recorded in polycrystalline diamond. *Science* 289, 1182–1185.

Jacob, D.E., Dobrzhinetskaya, L., Wirth, R. (2014) New insight into polycrystalline diamond genesis from modern nanoanalytical techniques. *Earth-Science Reviews* 136, 21–35.

Kaiser, W., Bond, W.L. (1959) Nitrogen, a major impurity in common type I diamond. *Physical Review Letters* 115, 857–863.

Kurat, G., Dobosi, G. (2000) Garnet and diopside-bearing diamondites (framesites). *Mineralogy and Petrology* 69, 143-159.

Mikhail, S., Kurat, G., Dubosi, G., Verchovsky, A.B., Jones, A.P., Mileage, H.J. (2013) Peridotitic and websteritic diamondites provide new information regarding mantle melting and metasomatism induced through the subduction of crustal volatiles. *Geochimica Cosmochimica et Acta* 107, 1–11.

Mikhail, S., Howell, D., Hutchison, M., Verchovsky, A.B., Warburton, P., Southworth, R., Thompson, A.R., Jones, A.P., Mileage, H.J. (2014) Constraining the internal variability of carbon and nitrogen isotopes in diamonds. *Chemical Geology* 366, 14–23.

Mikhail, S., McCubbin, F.M., Jenner, F.E., Shirey, S.B., Rumble, D., Bowden, R. (2019) Diamondites: Evidence for a distinct tectono-thermal diamond-forming event beneath the Kaapvaal craton. *Contributions to Mineralogy and Petrology* 174, 71.

Navon, O., Hutcheon, I.D., Rossman, G.R., Wasserburg, G.J. (1988) Mantle-derived fluids in diamond micro-inclusions. *Nature* 335, 784–789.

Porcelli, D., Elliott, T. (2008) The evolution of He Isotopes in the convecting mantle and the preservation of high ^{3}He/^{4}He ratios. *Earth and Planetary Science Letters* 269, 175–185.

Shirey, S.B., Cartigny, P., Frost, D.J., Keshav, S., Nestola, F., Nimis, P., Pearson, D.G., Sobolev, N.V., Walter, M.J. (2013) Diamonds and the geology of mantle carbon. *Reviews in Mineralogy and Geochemistry* 75, 355–421.

Smith, C.B., Walter, M.J., Bulanova, G.P., Mikhail, S., Burnham, A.D., Gobbo, L., Kohn, S.C. (2016). Diamonds from Dachine, French Guiana: a unique record of Early Proterozoic subduction. *Lithos* 265, 82–95.

Stuart, F.M., Lass-Evans, S., Fitton, J.G., Ellam, R.M. (2003) Extreme ^{3}He/^{4}He in picritic basalts from Baffin Island: role of a mixed reservoir in mantle plumes. *Nature* 424, 57–59.

Thomazo, C., Pinti, D.L., Busigny, V., Ader, M., Hashizume, K., Philippot, P. (2009) Biological activity and the Earth's surface evolution: Insights from carbon, sulfur, nitrogen and iron stable isotopes in the rock record. *Comptes Rendus Palevol* 8, 665–678.

Timmermann, S., Honda, M., Phillips, D., Jaques, A.L., Harris, J.W. (2018) Noble gas geochemistry of fluid inclusions in South African diamonds: implications for the origin of diamond-forming fluids. *Mineralogy and Petrology* 112, 181–195.

Timmermann, S., Yeowa, H., Honda, M., Howell, D., Jaquesa, A.L., Krebs, M.Y., Woodland, S., Pearson, D.G., Ávila, Y.A., Ireland, T.R. (2019a) U-Th/He systematics of fluid-rich 'fibrous' diamonds – Evidence for pre- and syn-kimberlite eruption ages. *Chemical Geology* 515, 22–36.

Timmerman, S., Honda, M., Burnham, A.D., Amelin, Y., Woodland, S., Pearson, D.G., Jaques, A.L., Le Losq, C., Bennett, V.C., Bulanova, G.P., Smith, C.B., Harris, J.W., Tohver. E. (2019b) Primordial and recycled helium isotope signatures in the mantle transition zone. *Science* 16, 692–694.

Torsvik, T., Burke, K., Steinberger, B., Webb, S.J., Ashwal, L. (2010) Diamonds sampled by plumes from the core-mantle boundary. *Nature* 466, 352–355.

Weiss, Y., McNeill, J., Pearson, D.G., Nowell, G.M., Ottley, C.J. (2015) Highly saline fluids from a subducting slab as the source for fluid-rich diamonds. *Nature* 524, 339–342.

Yakubovich, O., Stuart, F.M., Nesterenok, A., Carracedo, A.P. (2019) Cosmogenic ^{3}He in alluvial metal and alloy grains; assessing the potential as a tool for quantifying sediment transport times. *Chemical Geology* 517, 22–33.

Geochemical Perspectives Letters

A secretive mechanical exchange between mantle and crustal volatiles revealed by helium isotopes in ^{13}C-depleted diamonds

S. Mikhail, J.C. Crosby, F.M. Stuart, L. DiNicola, F.A.J. Abernethy

Supplementary Information

The Supplementary Information includes:

- Sample Descriptions
- Carbon and Nitrogen Isotope Analysis
- Helium Isotope Analysis
- Table S-1
- Supplementary Information References

Sample Descriptions

The Orapa diamondites originate from the largest of 23 pipes in the Orapa cluster in north-eastern Botswana, emplaced at 93.1 Ma on the western margin of the Kalahari Craton (samples described in Mikhail *et al*., 2019). The southern African diamondites were selected from a collection at the Naturhistorische Museum Vienna, Austria. Detailed descriptions of the samples are provided by Kurat and Dobosi (2000). Similar samples were described from the Orapa, Jwaneng (Botswana; Gurney and Boyd, 1982) and Venetia kimberlites (South Africa; Jacob *et al*., 2000). These samples likely originate from one or all these sources. The complete sample suite (Orapa + southern African diamondites) incorporates a range of silicate parageneses; five contain websteritic garnets, four contain eclogitic garnets, one shows a mixed paragenesis containing both peridotitic clinopyroxene (Mg# = 90.81) and an orange eclogitic garnet, and seven samples contain no paragenesis-defining intergrowths/inclusions (Table S-1).

Carbon and Nitrogen Isotope Analysis

The δ^{13}C-, δ^{15}N-values and N-concentrations were obtained using the custom-made fully automated Finesse machine at the Open University, UK (Verchovsky *et al*., 1998) following the method outlined in Mikhail *et al*. (2014). Samples analysis was undertaken using platinum sample buckets (99.95 % purity platinum foil of 0.025 mm thickness). A foil strip was cut and placed in a 6 mm ID quartz tube alongside a platinum-wrapped mass of copper oxide wire, then connected to the vacuum system of Finesse in order to evacuate the tube. After this process, the tube was torched off using a hydrogen-oxygen blowtorch, collapsing the glass in order to maintain vacuum, and placed overnight in a 900 °C muffle furnace. This has the effect of liberating oxygen from the breakdown of the copper oxide wire, which serves to oxidise and remove contamination from the foil. Once removed from the muffle furnace, the tube was allowed to cool before being opened in a class 100 clean room. The sample buckets themselves were produced but cutting subsections from the foil strip and folding them into the correct shape using cleaned scissors and tweezers within the clean room. Samples were weighed directly into the buckets using a Sartorius microbalance that had been zeroed to the mass of each platinum

bucket. Tweezers were used to place fragments of the samples into the buckets, after which they were weighed, closed and gently compacted then placed into Finesse sample inlet system.

Once within the furnace, the samples were step heated. The first two steps were cleaning steps, consisting of a single pyrolysis at 1100 °C followed by combustion at 500 °C, in order to remove any residual contaminants. Subsequently, samples are combusted at 1100 °C for as many steps as were required return the system to blank levels (*i.e.* complete oxidation of diamond). Oxygen gas (O_2) was derived from the breakdown of copper oxide wire in a separate linked furnace at 850 °C, with any residual oxygen at the end of each combustion step resorbed when the temperature of the CuO furnace dropped to 600 °C. The resultant gas was then passed through to a liquid nitrogen-cooled cold finger array and a molecular sieve, collectively separating and purifying the CO_2, N_2, H_2O, and noble gases. These were then separated by a valve before the cold finger was heated to approximately -50 °C in order to mobilise the CO_2 and transfer the gas to another liquid nitrogen-cooled cold finger attached to a 1 Torr MKS Baratron. Non-condensable gases were subsequently pumped away, the Baratron section isolated and the cold finger warmed to release the CO_2 for measurement on the Baratron. $\delta^{13}C$ was determined by a triple-collector magnetic sector mass spectrometer operating in static mode.

Following carbon analysis, the nitrogen was desorbed from the molecular sieve and cleaned using a secondary copper oxide source in order to remove any contribution from CO. An aliquot was sent to the quadrupole mass spectrometer in order to determine the N_2-abundance and to allow the system to determine and carry out a gas splitting procedure. The remaining gas was split and sent to the nitrogen mass spectrometer, again a triple collector magnetic sector instrument operating in static mode. The gas was purified by use of another cold finger adjacent to the mass spectrometer and used to remove any condensable gases. This provided both the $\delta^{15}N$ and the nitrogen abundance through a calculation based on the intensity of ^{14}N and the known volumes of the instrument.

Carbon and nitrogen stable isotope ratios ($^{13}C/^{12}C$ and $^{15}N/^{14}N$) are expressed in delta notation relative to the Pee Dee belemnite and air standards, respectively (*e.g.*, $\delta^{13}C$ = ($^{13}C/^{12}C$ sample / $^{13}C/^{12}C$ standard – 1)). The accuracy of the analysis determined by the analysis of the internal standards is ±<0.5 ‰ for $\delta^{13}C$ and $\delta^{15}N$ values and <10 % for the N concentrations (2σ). Carbon isotopic errors are determined as standard deviations of the reference materials. Nitrogen isotopic errors were determined using the statistical methodology outlined by Equations S-1 to S-3 (see Mikhail *et al.*, 2014).

$$Mass\ of\ nitrogen\ in\ the\ sample = N_m - N_b \qquad \text{Eq. S-1}$$

$$\delta^{15}N_c = \frac{(\delta^{15}N_m)-(\delta^{15}N_b \,.\, N_b)}{N_m - N_b} \qquad \text{Eq. S-2}$$

$$\Delta\delta^{15}N_c = \frac{1}{(N_m-N_b)^2} \cdot \sqrt{[(1-\delta^{15}N_m)^2.(\Delta N_m)^2 + (1-\delta^{15}N_b)^2.\,(N_m - N_b)^2\,.((\Delta N_m)^2.(\Delta\delta^{15}N_m)^2 + (\Delta N_b)^2.(\Delta\delta^{15}N_b)^2)]} \qquad \text{Eq. S-3}$$

where N_m and N_b refer to the mass of nitrogen in the measured gas and blank, $\delta^{15}N_m$ and $\delta^{15}N_b$ refer to the $\delta^{15}N$ value of the measured gas and blank, $\Delta\delta^{15}N_m$ refers to the measured error in per mil, $\Delta\delta^{15}N_b$ and ΔN_b refer to the standard deviation for the multiple blank analysis and $\Delta\delta^{15}N_c$ is the blank corrected precision of the $\delta^{15}N$ value of the sample.

Helium Isotope Analysis

Helium analyses for samples from Orapa were undertaken using a ThermoFisher Scientific Helix SFT dual collector mass spectrometer. Southern African samples were analysed using a MAP 215-50 all-metal magnetic sector mass spectrometer. Both analyses were undertaken at the Scottish Universities Environmental Research Centre following methods adapted from Stuart *et al.* (2000). Sample fragments were weighed using a Satorius MSE3.6P-000-DM Cubis Micro Balance and washed with acetone in an ultrasonic bath for 15 minutes at the University of St. Andrews. Samples were then loaded into an all-metal multi-sample hydraulic crusher. The gas trapped in fluid inclusions is released by *in vacuo* crushing and then purified in an all-metal ultra-high-vacuum line equipped with two heated (250 °C) SAES GP50 getters and one activated charcoal finger (cooled to approximately -196 °C using liquid nitrogen) for 15 minutes prior to expand into the mass spectrometer. The mass spectrometer is equipped with a SAES GP50 getter (operated at room temperature) and a stainless steel finger filled with activated charcoal (cooled to *ca.* -196 °C using liquid Nitrogen) installed close to the source to minimise partial pressure of residual gases during analysis. ^3He is analysed by a copper beryllium ion counting electron multiplier and ^4He is analysed by an electrically suppressed Faraday detector. Determination of mass spectrometer sensitivity and ratio reproducibility was performed measuring multiple times each day helium standard gas HESJ (Matsuda *et al.*, 2002) with $^3He/^4He$ ratio of 20.63 ± 0.10 R_A (R_A being the $^3He/^4He$ ratio of air 1.34 x 10^{-6},

Mishima *et al.*, 2018) and blank analyses were frequently run to obtain a well constrained background level of ^{3}He and ^{4}He. The average blank levels of the ThermoFisher Scientific Helix SFT are $4.21 \times 10^{-12} \pm 2.89 \times 10^{-12}$ cm^3 for ^{4}He and $6.68 \times 10^{-16} \pm 1.59 \times 10^{-16}$ cm^3 for ^{3}He. The average blank levels of the MAP 215-50 are $7.52 \times 10^{-11} \pm 8.06 \times 10^{-12}$ cm^3 for ^{4}He and $1.17 \times 10^{-15} \pm 1.25 \times 10^{-15}$ cm^3 for ^{3}He.

The intensity of the ion beams of both ^{3}He and ^{4}He are measured simultaneously in a 20-cycle run setup using Qtegra software. The ^{3}He and ^{4}He abundance of each sample was calculated by taking the average of these 20 cycles and the uncertainty is the standard deviation. The blank corrected $^{3}He/^{4}He$ isotopic ratios of each sample (R) are expressed relative to the $^{3}He/^{4}He$ of air ($R_a = 1.34 \times 10^{-6}$; Mishima *et al.*, 2018) as R/R_a using the internal HESJ standard.

Table S-1 Full dataset used in this study.

Source of Data		Location	Type	Paragenesis	Minerals	R/Ra New	±	^{4}He ccSTP/g	^{4}He bulk	^{4}He bulk error	^{3}He ccSTP/g	^{3}He bulk	^{3}He bulk error	δ^{13}C	±	N at. ppm	δ^{15}N	±
This study	DIA030	Southern Africa	Polycrystalline	Websteritic	Garnet	8.51	0.42	1.330E-07	4.456E-09	1.742E-11	1.506E-12	4.857E-14	2.714E-15	-16.6	0.2	8	+6.4	3.9
This study	DIA053	Southern Africa	Polycrystalline	Websteritic	Garnet	2.76	0.70	3.200E-08	9.075E-10	1.358E-11	1.177E-13	2.409E-15	1.691E-15	-20.8	0.5	56	+2.0	0.7
This study	DIA057B#1	Southern Africa	Polycrystalline	Unknown	None characteristic	0.06	0.05	6.790E-07	1.696E-08	6.857E-11	5.810E-14	2.107E-16	1.782E-15	-21.4	0.1	1389		
This study	DIA057B#2	Southern Africa	Polycrystalline	Unknown	None characteristic	0.14	0.05	6.900E-07	1.725E-08	5.846E-11	1.247E-13	1.676E-15	1.783E-15	-21.4	0.1	1389		
This study	DIA058B	Southern Africa	Polycrystalline	Eclogitic	Orange Garnet	3.89	0.21	7.420E-08	7.835E-09	3.339E-11	3.841E-13	4.066E-14	2.526E-15	-19.1	0.1			
This study	DIA059	Southern Africa	Polycrystalline	Websteritic	Garnet	0.53	0.20	1.420E-07	4.218E-09	1.740E-11	1.007E-13	1.676E-15	1.690E-15	-22.2	0.3	13	+5.3	6.1
This study	DIA073B	Southern Africa	Polycrystalline	Websteritic	Garnet	1.91	0.40	8.710E-08	4.008E-09	1.759E-11	2.210E-13	8.710E-15	2.461E-15	-17.4	0.1	2812	+6.9	0.5
This study	DIA077	Southern Africa	Polycrystalline	Unknown	None characteristic	7.44	0.54	1.440E-07	5.934E-09	2.211E-11	1.425E-12	5.941E-14	4.414E-15					
This study	ORF9	Orapa, Bostwana	Polycrystalline	Webesteritic	Garnet			2.441E-08						-5.3	0.1			
This study	ORF12	Orapa, Bostwana	Polycrystalline	Unknown	None characteristic			6.725E-08										
This study	ORF19	Orapa, Bostwana	Polycrystalline	Ecologitic	Orange Garnet	4.22	2.72	9.021E-08	1.911E-10	1.159E-11	5.110E-13	1.082E-15	7.265E-16	-8.0	0.1	255	+5.8	0.1
This study	ORF26#1	Orapa, Bostwana	Polycrystalline	Peridotitic & Eclogitic	Clinopyroxene & Garnet			4.220E-09	1.006E-11	3.787E-12				-14.6	0.2	38	-4.9	2.2
This study	ORF26#2	Orapa, Bostwana	Polycrystalline	Peridotitic & Eclogitic	Clinopyroxene & Garnet				1.006E-11	3.787E-12				-17.8	0.2	19	+23.2	6.6
This study	ORF28#1	Orapa, Bostwana	Polycrystalline	Unknown	None characteristic			5.368E-08						-4.3	0.1	775	+2.9	0.2
This study	ORF28#2	Orapa, Bostwana	Polycrystalline	Unknown	None characteristic				1.137E-10	7.512E-12		2.390E-16	4.448E-16	-4.9	0.2	52	+19.7	0.6
This study	ORF41	Orapa, Bostwana	Polycrystalline	Unknown	None characteristic			7.766E-08						-14.8	0.3	1146	+14.7	0.2
This study	ORF57	Orapa, Bostwana	Polycrystalline	Eclogitic	Orange Garnet	7.53	0.75	2.238E-07	1.586E-09	8.884E-11	2.259E-12	1.602E-14	1.921E-15	-16.6	0.2	17	+18.4	3.0
This study	ORF60	Orapa, Bostwana	Polycrystalline	Unknown	Chromite				0.000E+00	0.000E+00		0.000E+00	0.000E+00	-6.5	0.1	1054	+12.1	0.2
This study	ORF91	Orapa, Bostwana	Polycrystalline	Unknown	None characteristic									-20.3	0.3	401	+4.4	0.3

This study	ORF143	Orapa, Bostwana	Polycrystalline	Ecologitic	Orange Garnet	1.58	1.12	1.027E-07	4.400E-10	2.482E-11	2.174E-13	9.317E-16	6.858E-16	-19.9	0.2	647	+10.0	0.2
Gautheron et *al.*, 2005	ORPC 1	Orapa, Botswana	Polycrystalline	Eclogitic	Orange Garnet	0.56	0.06	4.620E-07	1.983E-07	7.296E-11	1.482E-13	6.360E-14		-14.0	0.1	202	+4.5	0.5
Gautheron et *al.*, 2005	ORPC 2	Orapa, Botswana	Polycrystalline	Eclogitic	Orange Garnet	1.34	0.11	1.490E-07	9.615E-08	4.517E-11	1.717E-13	1.108E-13		-21.0	0.1	543	+15.5	0.5
Gautheron et *al.*, 2005	ORPC 3	Orapa, Botswana	Polycrystalline	Eclogitic	Orange Garnet	0.43	0.04	3.010E-07	1.655E-07	1.803E-09	9.391E-14	5.163E-14		-19.4	0.1	163	+6.7	0.5
Gautheron et *al.*, 2005	ORPC 4 #1	Orapa, Botswana	Polycrystalline	Peridotitic	Enerald-Green Diopside	0.97	0.04	6.620E-07	4.572E-07	1.520E-10	5.949E-13	4.109E-13		-9.8	0.1	1973	+8.1	0.5
Gautheron et *al.*, 2005	ORPC 4 #2	Orapa, Botswana	Polycrystalline	Peridotitic	Enerald-Green Diopside	0.15	0.05	1.090E-06	2.476E-07	9.088E-12	4.798E-14	1.090E-14						
Gautheron et *al.*, 2005	ORPC 5	Orapa, Botswana	Polycrystalline	Unknown	None Characteristic	0.86	0.08	2.180E-07	1.240E-07	1.536E-10	1.425E-13	8.108E-14		-18.3	0.1	69	+8.1	0.5
Gautheron et *al.*, 2005	ORPC 6	Orapa, Botswana	Polycrystalline	Unknown	None Characteristic	0.54	0.04	5.430E-07	4.381E-07	7.552E-09	3.153E-13	2.544E-13		-21.0	0.1	168	+6.7	0.5
Burgess *et al.*, 1998	Jwaneng 3	Jwaneng, Botswana	Polycrystalline	Unknown	None Distinctive	4.46	0.10	2.480E-06			1.476E-11			-21.7	0.1			
Burgess *et al.*, 1998	Jwaneng 5	Jwaneng, Botswana	Polycrystalline	Unknown	None Distinctive									-5.5	0.1			
Burgess *et al.*, 1998	Jwaneng F6	Jwaneng, Botswana	Polycrystalline	Unknown	None Distinctive	0.18	0.00							-23.6	0.1			
Burgess *et al.*, 1998	Jwaneng F10	Jwaneng, Botswana	Polycrystalline	Unknown	None Distinctive	0.12	0.00							-23.6	0.1			
Burgess *et al.*, 1998	Jwaneng F11	Jwaneng, Botswana	Polycrystalline	Unknown	None Distinctive	0.13	0.01							-20.1	0.1			
Burgess *et al.*, 1998	Orapa 1	Orapa, Botswana	Polycrystalline	Eclogitic	Garnet	2.00	0.05	3.300E-07			8.815E-13			-18.6	0.1			
Burgess *et al.*, 1998	Orapa 2	Orapa, Botswana	Polycrystalline	Eclogitic	Garnet	1.97	0.04	3.000E-08			7.889E-14			-5.3	0.1			
Burgess *et al.*, 1998	Orapa 3	Orapa, Botswana	Polycrystalline	Eclogitic	Garnet	0.08	0.00				7.274E-12			-20.1	0.1			
Burgess *et al.*, 1998	Orapa 4	Orapa, Botswana	Polycrystalline	Eclogitic	Garnet	1.29	0.04	2.600E-07			4.462E-13			-9.6	0.1			
Burgess *et al.*, 1998	Orapa 5	Orapa, Botswana	Polycrystalline	Eclogitic	Garnet	1.38	0.02	2.200E-07			4.050E-13			-9.7	0.1			
Burgess *et al.*, 1998	Orapa F121	Orapa, Botswana	Polycrystalline	Eclogitic	Garnet	1.08	0.07				0.000E+00			-22.5	0.1			
Burgess *et al.*, 1998	Jwaneng 1	Jwaneng, Botswana	Coated	Unknown	None Distinctive	4.25	0.20	2.560E-06			1.453E-11			-5.9	0.1			
Burgess *et al.*, 1998	Jwaneng 2	Jwaneng, Botswana	Coated	Unknown	None Distinctive	3.84	0.10	3.220E-06			1.649E-11			-6.3	0.1			
Burgess *et al.*, 1998	Jwaneng 4	Jwaneng, Botswana	Coated	Unknown	None Distinctive	5.91	0.10	2.130E-06			1.680E-11			-6.6	0.1			

Burgess *et al.*, 1998	Jwaneng 6	Jwaneng, Botswana	Coated	Unknown	None Distinctive									-8.2	0.1			
Burgess *et al.*, 1998	Jwaneng 88	Jwaneng, Botswana	Coated	Unknown	None Distinctive	6.64	0.10	2.600E-07			2.303E-12			-5.3	0.1			
Burgess *et al.*, 1998	Jwaneng 89	Jwaneng, Botswana	Coated	Unknown	None Distinctive	7.26	0.20	1.540E-06			1.492E-11			-5.6	0.1			
Burgess *et al.*, 1998	Jwaneng 90	Jwaneng, Botswana	Coated	Unknown	None Distinctive	7.26	0.20	1.860E-06			1.802E-11			-5.4	0.1			
Burgess *et al.*, 1998	Jwaneng 112	Jwaneng, Botswana	Coated	Unknown	None Distinctive									-5.1	0.1			
Burgess *et al.*, 1998	DBP 7	DeBeers Pool, South Africa	Cloud	Unknown	None Distinctive	4.67	0.00								0.1			
Burgess *et al.*, 1998	Finsch 4	Finsch, South Africa	Cloud	Unknown	None Distinctive	3.73	0.30							-4.4	0.1			
Burgess *et al.*, 1998	Premier 2	Premier, South Africa	Cloud	Unknown	None Distinctive	3.53	0.20							-4.9	0.1			
Burgess *et al.*, 1998	Premier 4	Premier, South Africa	Cloud	Unknown	None Distinctive									-5.4	0.1			
Burgess *et al.*, 1998	Premier 8	Premier, South Africa	Cloud	Unknown	None Distinctive	0.31	0.00							-4.8	0.1			
Timmermann *et al.*, 2018	Fin1a	Finsch, South Africa	Coated	Unknown	None Distinctive									-6.3		640		
Timmermann *et al.*, 2018	Fin1b	Finsch, South Africa	Coated	Unknown	None Distinctive			7.310E-07	2.127E-08	1.804E-10				-6.2		750		
Timmermann *et al.*, 2018	Fin02	Finsch, South Africa	Coated	Unknown	None Distinctive	6.94	0.15	4.140E-06	3.304E-07	2.729E-09	3.930E-11	3.136E-12	6.799E-14	-5.1				
Timmermann *et al.*, 2018	Fin03	Finsch, South Africa	Coated	Unknown	None Distinctive	3.37	0.82	3.490E-07	1.661E-08	1.461E-10	1.610E-12	7.664E-14	1.928E-14	-3.4		30		
Timmermann *et al.*, 2018	DBP06	DeBeers Pool, South Africa	Coated	Unknown	None Distinctive	4.85	0.10	6.510E-06	3.242E-07	2.674E-09	4.330E-11	2.156E-12	4.656E-14	-6.7				
Timmermann *et al.*, 2018	DBP07	DeBeers Pool, South Africa	Coated		Saline HDF + Carbonate	3.99	0.08	2.050E-05	7.462E-07	6.188E-09	1.120E-10	4.077E-12	8.736E-14	-4.4		330		
Timmermann *et al.*, 2018	DBP08a	DeBeers Pool, South Africa	Coated	Unknown	None Distinctive	5.34	0.11	1.740E-05	6.577E-07	5.405E-09	1.270E-10	4.801E-12	1.013E-13	-7.1				
Timmermann *et al.*, 2018	DBP08b	DeBeers Pool, South Africa	Coated	Unknown	None Distinctive	5.17	0.15	1.040E-05	1.841E-07	1.512E-09	7.380E-11	1.306E-12	3.859E-14	-7.6				
Timmermann *et al.*, 2018	DBP09a	DeBeers Pool, South Africa	Coated	Unknown	None Distinctive	3.89	0.13	1.660E-05	1.262E-07	1.034E-09	8.810E-11	6.696E-13	2.341E-14	-6.6				
Timmermann *et al.*, 2018	DBP09b	DeBeers Pool, South Africa	Coated	Unknown	None Distinctive	5.07	0.18	7.170E-06	1.542E-07	1.273E-09	4.980E-11	1.071E-12	3.892E-14	-6.4				
Timmermann *et al.*, 2018	DBP09c	DeBeers Pool, South Africa	Coated	Unknown	None Distinctive	4.84	0.12	1.020E-05	3.050E-07	2.509E-09	6.740E-11	2.015E-12	5.173E-14	-6.6				
Timmermann *et al.*, 2018	DBP10a	DeBeers Pool, South Africa	Coated	Lherzolite	Olivine			3.360E-06	4.234E-08	3.843E-10				-5.1		470		

Timmermann *et al.*, 2018	DBP10b	DeBeers Pool, South Africa	Coated	Lherzolite	Olivine	5.05	0.14	5.700E-06	1.733E-07	1.426E-09	3.940E-11	1.198E-12	3.344E-14	-8.1		520		
Timmermann *et al.*, 2018	DBP14	DeBeers Pool, South Africa	Coated	Peridotitic & Websteritic	Olivine & Enstatite	5.01	0.10	2.490E-05	1.820E-06	1.499E-08	1.710E-10	1.250E-11	2.646E-13	-6.9				
Timmermann *et al.*, 2018	DBP15a	DeBeers Pool, South Africa	Coated	Peridotitic	Enstatite	2.01	0.04	6.510E-05	2.038E-06	1.681E-08	1.790E-10	5.603E-12	1.233E-13	-5.9				
Timmermann *et al.*, 2018	DBP15b	DeBeers Pool, South Africa	Coated	Peridotitic	Enstatite	4.08	0.09	1.690E-05	4.293E-07	3.531E-09	9.420E-11	2.393E-12	5.461E-14	-6.3				
Timmermann *et al.*, 2018	DBP15c	DeBeers Pool, South Africa	Coated	Peridotitic	Enstatite	4.40	0.10	1.950E-05	3.861E-07	3.168E-09	1.180E-10	2.336E-12	5.366E-14	-5.9				
Timmermann *et al.*, 2018	KOF17a	Koffiefontein, South Africa	Coated		Calcite	4.76	0.26	2.470E-06	3.977E-08	3.284E-10	1.610E-11	2.592E-13	1.481E-14	-4.9		800		
Timmermann *et al.*, 2018	KOF17b	Koffiefontein, South Africa	Coated		Calcite			1.670E-06	5.828E-08	4.816E-10				-4.9		500		
Timmermann *et al.*, 2018	KOB18a	Koffiefontein, South Africa	Coated	Peridotitic	Peridotitic Sulphide	4.97	0.18	1.970E-06	1.178E-07	9.688E-10	1.340E-11	8.013E-13	2.948E-14	-5.4		510		
Timmermann *et al.*, 2018	KOB18b	Koffiefontein, South Africa	Coated	Peridotitic	Peridotitic Sulphide	5.90	0.67	5.460E-07	1.714E-08	1.473E-10	4.410E-12	1.385E-13	1.630E-14	-5.5		450		
Timmermann *et al.*, 2018	KOB19a	Koffiefontein, South Africa	Coated		Saline HDF + Carbonate	5.82	0.25	1.130E-06	4.125E-08	3.405E-10	8.970E-12	3.274E-13	1.467E-14	-6.4		620		
Timmermann *et al.*, 2018	KOF19b	Koffiefontein, South Africa	Coated		Saline HDF + Carbonate	5.22	0.66	2.530E-07	1.369E-08	1.190E-10	1.810E-12	9.792E-14	1.288E-14	-6.4		540		
Timmermann *et al.*, 2019	409b	Jwaneng, Botswana	Coated		Eclogitic	0.16	0.00	6.710E-07	7.059E-08	7.580E-10	1.390E-13	1.461E-14	1.570E-16	-6.8		900		
Timmermann *et al.*, 2019	410A	Jwaneng, Botswana	Coated		Eclogitic	1.92	0.54	8.830E-07	1.678E-08	4.900E-09	2.250E-12	4.283E-14	1.250E-14	-6.2		140		

Supplementary Information References

Burgess, R., Johnson, L., Mattey, D., Harris, J., Turner, G. (1998) He, Ar and C isotopes in coated and polycrystalline diamonds. *Chemical Geology* 146, 205–217.

Gautheron, C., Cartigny, P., Moreira, M., Harris, J., Allegre, C. (2005) Evidence for a mantle component shown by rare gases, C and N isotopes in polycrystalline diamonds from Orapa (Botswana). *Earth and Planetary Science Letters* 240, 559–572.

Gurney J. J., Boyd F. R. (1982) Mineral intergrowths with polycrystalline diamonds from Orapa Mine, Botswana. *Carnegie Institution of Washington Yearbook* 81, 267–273.

Jacob, D.E., Viljoen, K.S., Grassineau, N., Jagoutz, E. (2000) Remobilization in the Cratonic Lithosphere Recorded in Polycrystalline Diamond. *Science* 289, 1182-1185.

Kurat, G., Dobosi, G. (2000) Garnet and diopside-bearing diamondites (framesites). *Mineralogy and Petrology* 69, 143-159.

Matsuda, J., Matsumoto, T., Sumino, H., Nagao, K., Yamamoto, J., Miura, Y., Sano, Y. (2002) The 3He/4He ratio of the new internal He Standard of Japan (HESJ). *Geochemical Journal* 36, 191–195.

Mikhail, S., Verchovsky, A.B., Howell, D., Hutchison, M.T., Southworth, R., Thomson, A.R., Warburton, P., Jones, A.P., Milledge, H.J. (2014) Constraining the internal variability of the stable isotopes of carbon and nitrogen within mantle diamonds. *Chemical Geology* 366, 14–23.

Mikhail, S., McCubbin, F.M., Jenner, F.E., Shirey, S.B., Rumble, D., Bowden, R. (2019) Diamondites: Evidence for a distinct tectono-thermal diamond-forming event beneath the Kaapvaal craton. *Contributions to Mineralogy and Petrology* 174, 71.

Mishima, K., Sumino, H., Yamada, T., Leki, S., Nagakura, N., Hidetoshi, O., Oide, H. (2018) Accurate Determination of the Absolute 3He/4He Ratio of a Synthesized Helium Standard Gas (Helium Standard of Japan, HESJ): Toward Revision of the Atmospheric 3He/4He Ratio. *Geochemistry, Geophysics, Geosystems* 19, 3995-4005.

Stuart, F.M., Ellam, R.M., Harrop, P.J., Fitton, J.G., Bell, B.R. (2000) Constraints on mantle plumes from the helium isotopic composition of basalts from the British Tertiary Igneous Province. *Earth and Planetary Science Letters* 177, 273–285.

Timmermann, S., Honda, M., Phillips, D., Jaques, A.L., Harris, J.W. (2018) Noble gas geochemistry of fluid inclusions in South African diamonds: implications for the origin of diamond-forming fluids. *Mineralogy and Petrology* 112, 181–195.

Timmermann, S., Yeowa, H., Honda, M., Howell, D., Jaquesa, A.L., Krebs, M.Y., Woodland, S., Pearson, D.G., Ávila, Y.A., Ireland, T.R. (2019) U-Th/He systematics of fluid-rich 'fibrous' diamonds – Evidence for pre- and syn-kimberlite eruption ages. *Chemical Geology* 515, 22–36

Verchovsky, A.B., Fisenko, A.V., Semjonova, L.F., Wright, I.P., Lee, M.R. and Pillinger, C.T. (1998) C, N, and noble gas isotopes in grain size separates of presolar diamonds from Efremovka. *Science* 281, 1165–1168.